Mainz Microtron MAMI

Collaboration A1: "Virtual Photons"

Spokesperson: H. Merkel

Proposal for an Experiment

**A study of the Q^2-dependence
of the structure functions $P_{LL} - P_{TT}/\epsilon$ and P_{LT}
and the generalized polarizabilities α_E and β_M
in Virtual Compton Scattering at MAMI**

Collaborators:

P. Achenbach, C. Ayerbe Gayoso, J. C. Bernauer, R. Böhm, A. Denig,
M. O. Distler, A. Esser, M. Gómez Rodríguez, K. Grießinger, F. E. Maas, H. Merkel*,
U. Müller, L. Nungesser, J. Pochodzalla, T. R. Saito, S. Sánchez Majos,
B. S. Schlimme, M. Weinriefer
(Institut für Kernphysik, Universität Mainz)

C. Muñoz Camacho, H. Fonvieille*
(LPC IN2P3-CNRS, Université Blaise Pascal, Clermont-Ferrand, France)

L. Debenjak, M. Potokar, S. Širca
(University of Ljubljana and Institut "Jožef Stefan" Ljubljana, Slovenia)

D. Bosnar, I. Friščić, M. Makek
(Department of Physics, University of Zagreb, Croatia)

B. Pasquini
(Universitá degli Studi di Pavia and INFN, Sezione di Pavia, Pavia, Italy)

*Contact Person (E-Mail: helene@clermont.in2p3.fr, merkel@kph.uni-mainz.de)

Abstract

The Generalized Polarizabilities (GPs) are fundamental quantities characterizing the electromagnetic structure of a nucleon that is deformed by an external quasi-static electromagnetic field. These observables are accessed in Virtual Compton Scattering (VCS).

A series of experiments of the type $ep \to ep\gamma$ have been performed, at Bates, MAMI and JLab, in order to investigate the behavior of the electric and magnetic GPs of the proton, α_E and β_M, as a function of Q^2 or the distance scale. These GPs are contained in the two structure functions, $P_{LL} - P_{TT}/\epsilon$ and P_{LT}, that enter the unpolarized $ep \to ep\gamma$ cross section.

The overall experimental picture indicates a non-trivial Q^2-behavior of these VCS observables, and we propose to investigate the subject in further details. We propose to study the $ep \to ep\gamma$ reaction at three different Q^2: 0.1, 0.2 and 0.5 GeV^2, where there are no experimental data. The unpolarized cross section will be measured below the pion production threshold, with the electron beam at MAMI-C energies, using the A1 detector setup and the hydrogen target. We plan to use two analysis techniques, in order to produce the most complete set of data for the physics observables. High statistics will ensure competitive error bars. The total beamtime requested is about 800 hours.

These new data will be an essential piece to build a consistent picture of the Q^2-dependence of the VCS structure functions and the GPs, to constrain the theoretical models and ultimately improve our understanding of the nucleon electromagnetic structure.

1   Introduction

1.1   An overview of VCS at low energy

The nucleon electromagnetic polarizabilities are well known, from Real Compton Scattering (RCS) on the nucleon $\gamma N \to \gamma N$. These fundamental observables tell us how the internal structure of the nucleon is deformed in an applied electromagnetic field. The measured values of the electric and magnetic proton polarizabilities $\alpha_E = (12.1 \pm 0.3_{stat} \pm 0.5_{syst})10^{-4}$ fm^3, $\beta_M = (1.6 \pm 0.4_{stat} \pm 0.6_{syst})10^{-4}$ fm^3 [1] show the extreme stiffness of the proton: this is a direct consequence of the strong binding of its inner constituents, the quarks and gluons.

The concept of polarizability goes one step further: these observables depend on the distance scale [2, 3] or equivalently the four-momentum transfer Q^2. They are then called Generalized Polarizabilities (GPs). As an example, just as the electric form factor G_E is the Fourier transform of the charge distribution inside the nucleon, the electric GP $\alpha_E(Q^2)$ is the Fourier transform of the modification of this charge distribution when the nucleon is surrounded by a static EM field. The GPs are thus of great interest to test QCD, essentially in its non-perturbative regime.

Low-energy Virtual Compton Scattering (VCS) $\gamma^* p \to \gamma p$ allows to access the GPs. A series of dedicated VCS experiments on the proton have been performed at various laboratories: MAMI [4, 5], Bates [6], Jlab [7]. After a little more than a decade of measurements, a picture emerges for the electric and magnetic GPs which can be confronted to the theory. Among the theoretical calculations of the GPs we find the Constituent Quark models [3, 8, 9], Linear Sigma model [10, 11], Effective Lagrangian [12, 13], Heavy Baryon Chiral Perturbation Theory (HBChPT) [14, 15, 16, 17, 18], Fully Covariant ChPT [19], and Dispersion Relations (DR) [20, 21]. We will essentially refer to HBChPT and DR, which have provided most of the developments in the field up to now. Reviews on VCS at low energy can be found in refs. [22, 23].

1.2   The photon electroproduction process

VCS on the proton is performed by exclusive photon electroproduction $ep \to ep\gamma$. Kinematics are defined by five independent variables, e.g. $(k_{lab}, k'_{lab}, \theta'_e, \theta_{\gamma\gamma cm}, \phi)$ or $(q_{cm}, q'_{cm}, \epsilon, \theta_{\gamma\gamma cm}, \phi)$, where k_{lab} and k'_{lab} are the incoming and final electron energies, θ'_e the scattered electron angle, $(\theta_{\gamma\gamma cm}, \phi)$ the polar and azimuthal angles of the Compton subprocess in its center-of-mass (CM), see Fig. 1. q_{cm} and q'_{cm} are the modulus of the initial and final photon three-momenta in the CM, and ϵ is the usual virtual photon polarization parameter.

The photon electroproduction amplitude is the coherent sum of the Bethe-Heitler, Born and non-Born contributions: see Fig. 2-left. The Bethe-Heitler and Born amplitudes are known and depend only on the elastic form factors G_E^p, G_M^p. The sum of these two amplitudes is noted (BH+B). The non-Born amplitude is the unknown part. At low energy it is parametrized by the GPs.
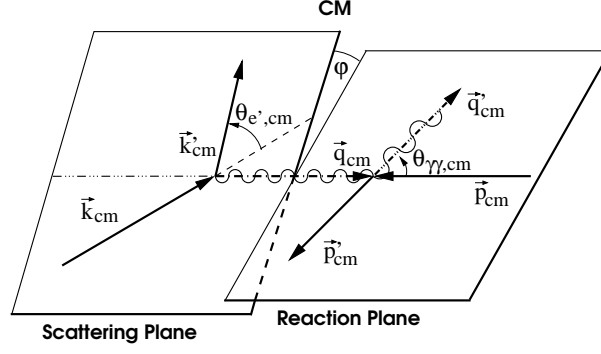
Figure 1: *Kinematics of the photon electroproduction reaction in the γp center-of-mass.*
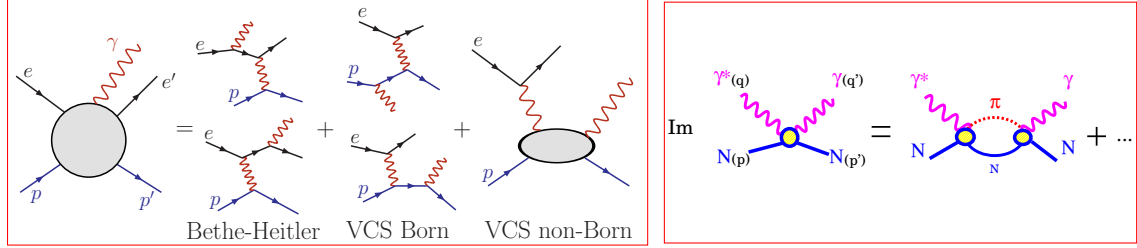
Figure 2: *Left: the various contributions to the photon electroproduction amplitude. Right: the imaginary part of the VCS amplitude in the formalism of Dispersion Relations.*

1.3   Analysis techniques for VCS

There are two techniques which allow to extract information on the GPs from a VCS measurement. They are briefly described below.

• Low-energy expansion or LEX analysis

An expansion in powers of q'_{cm}, or low-energy theorem, provides the main following result for the unpolarized photon electroproduction cross section [3] :

$$d^5\sigma(ep\gamma) = d^5\sigma_{BH+B} + (\Phi q'_{cm}) \times \left[v_{LL} \cdot (P_{LL} - P_{TT}/\epsilon) + v_{LT} \cdot (P_{LT}) \right] + \mathcal{O}(q'^{2}_{cm}) \tag{1}$$

where $d^5\sigma$ stands for $d^5\sigma/dk'_{lab}d\Omega'_{elab}d\Omega_{\gamma cm}$ and Φ, v_{LL}, v_{LT} are kinematical factors (see [24] for full details). This expansion is valid only below the pion production threshold. The Bethe-Heitler+Born cross section $d^5\sigma_{BH+B}$ is a known cross section, which contains no polarizability effect. In the formula two structure functions (or response functions) appear, which are linear combinations of GPs:

$$
\begin{aligned}
P_{LL} - P_{TT}/\epsilon &= & \frac{4M_p}{\alpha}G^p_E(Q^2) \cdot \alpha_E(Q^2) &+& [\text{spin-flip GPs}] \\
P_{LT} &= & -\frac{2M_p}{\alpha}\sqrt{\frac{q^2_{cm}}{Q^2}}G^p_E(Q^2) \cdot \beta_M(Q^2) &+& [\text{spin-flip GPs}]
\end{aligned}
\tag{2}
$$

(M_p = the proton mass and $\alpha = 1/137$). Truncating this expansion to the order q'_{cm}, i.e. neglecting the higher-order term $\mathcal{O}(q'^{2}_{cm})$, the structure functions $P_{LL} - P_{TT}/\epsilon$ and P_{LT} can be determined directly by measuring the *deviation* of

the experimental cross section from the (BH+B) cross section. The electric and magnetic GPs can be further extracted if one fixes the spin-flip GPs in eq. 2, for example using some theoretical model (these spin-flip GPs are basically unconstrained by existing measurements).

   • **Dispersion Relations or DR analysis**

Contrary to the LEX approach, in the DR formalism for VCS [20, 21] all orders in q'_{cm} are included, therefore the calculation is valid even above the pion production threshold. The VCS amplitude is given by s-channel dispersion integrals, in which the imaginary part is calculated through unitarity. The contribution from πN intermediate states, see Fig. 2-right, is calculated using the MAID multipoles [25].

In the DR model all first-order GPs are predicted, except two of them which are unconstrained: the electric and magnetic GPs. α_E and β_M are described through free parameters called Λ_α and Λ_β. Using this specific feature of the model, the electric and magnetic GPs as well as the structure functions $P_{LL} - P_{TT}/\epsilon$ and P_{LT} can be extracted most directly from an experiment, by just fitting the free parameters Λ_α and Λ_β to the measured $(ep \to ep\gamma)$ cross section.

1.4   World data on VCS unpolarized observables
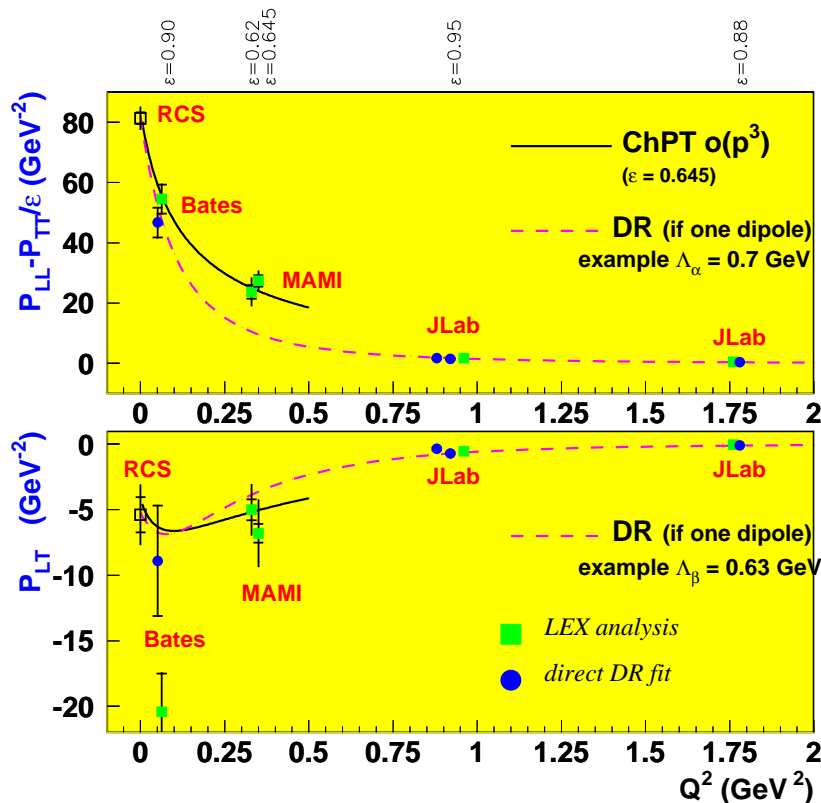
Figure 3: *World data on the VCS structure functions. The point at $Q^2 = 0$ is obtained from RCS [1]. The other points have been measured in VCS at Bates [6], MAMI [4, 5] and JLab [7]. The inner (resp. outer) error bar is statistical (resp. total). The value of ϵ of each experiment is indicated above the top plot. See text for the curves.*

3
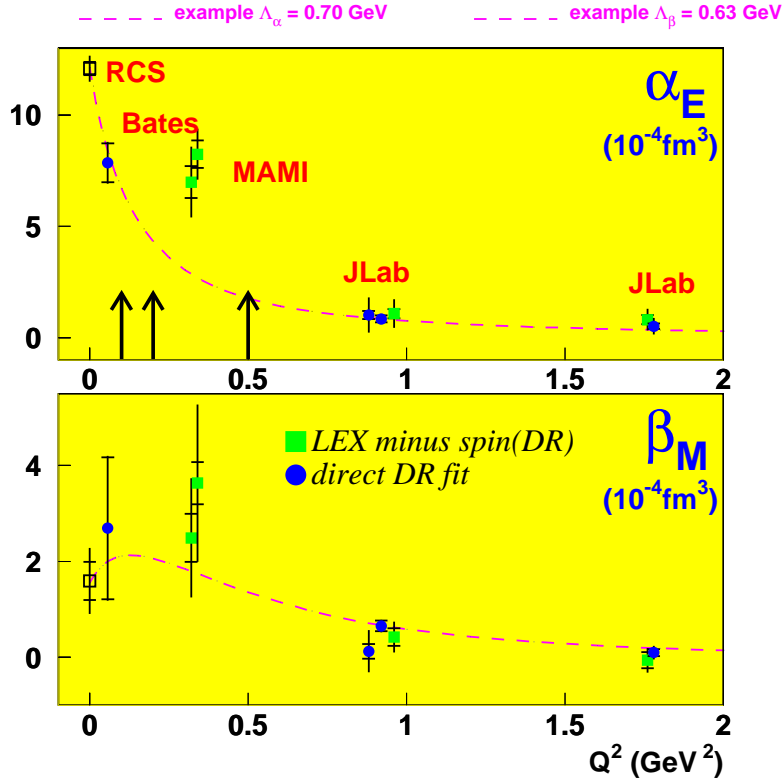
Figure 4: *World data on the electric GP (top) and magnetic GP (bottom). Same experiments as in the previous figure and same convention for the error bars. The arrows in the upper plot indicate the values of Q^2 at which we propose to make the measurements.*

The measurements have been made from low Q^2 (0.06 GeV^2 at Bates [6]) up to 0.9 and 1.8 GeV^2 at JLab [7]. The MAMI measurements [4, 5] were up to now concentrated at $Q^2 = 0.33$ GeV^2.

Fig. 3 shows our present knowledge of the structure functions $P_{LL} - P_{TT}/\epsilon$ and P_{LT}. The green and blue points are obtained according to LEX and DR analyses respectively, along the lines explained in section 1.3. Eq. 2 tells us that, up to a small term containing the spin-flip GPs, these structure functions are proportional to α_E and β_M, therefore they give an almost direct image of the electric and magnetic GPs.

The structure function $P_{LL} - P_{TT}/\epsilon$ in Fig. 3 falls rather smoothly with Q^2. The data agree well with the HBChPT calculation (black solid curve) at order p^3, in the low-Q^2 region where the theory is applicable. The Dispersion Relations have no such limitation in Q^2. The dashed magenta curve is an example of DR calculation, assuming one single dipole shape for the unconstrained part of the GPs. Here the free parameters Λ_α and Λ_β have been adjusted to the JLab data, and obviously it is not possible to account for all the data points with one single dipole shape.

The structure function P_{LT} takes small values, due to the smallness of β_M. This is traditionally explained by the interplay of the paramagnetic and diamagnetic contributions to β_M, which almost cancel at low Q^2 and also create an turn-over point, as can be seen in the two theoretical curves in Fig. 3-bottom. One will note

4

that this turn-over region is rather poorly known experimentally.

Fig. 4 shows the extraction of the electric and magnetic GPs from the same set of experiments. As mentioned in section 1.3, the DR extraction is made directly from the cross section data, while in the LEX method one has to subtract from the measured structure functions the spin-flip part. Here this is done using the DR model, and this is labelled "LEX minus spin(DR)" on Fig. 4.

All models predict a Q^2-behavior of the electric GP that is a single dipole, or very close. The observed fall-off of α_E *over the whole measured range* is strikingly different from this prediction. The data suggest that there is an enhancement at low Q^2, evidenced by the MAMI points at $Q^2 = 0.33$ GeV^2. More data points in this region are clearly needed to confirm this unexpected feature, and this is one goal of the proposal. Interpretations of such a possible "structure" in α_E are open. It could be due to the contribution of some specific resonances in the polarizabilities. It could also be due to the meson cloud surrounding the nucleon. Such mesonic effects have been invoked to interpret the low-Q^2 behavior of the nucleon form factors [26] and they could manifest themselves in the polarizabilities in an enhanced way.

The magnetic GP is smaller than α_E and more difficult to measure. It is very sensitive to systematic errors like absolute normalization, etc. The second goal of the proposal is to provide accurate data points for β_M at low Q^2, in the region of the turn-over, in order to better quantify the balance between diamagnetism and paramagnetism in the proton.

2   Goal of the proposed experiment

We propose to further explore the Q^2-dependence of the VCS unpolarized observables in the low-Q^2 domain. We plan to perform high-precision measurements of the unpolarized cross section of the process $ep \to ep\gamma$ at $Q^2 =0.1$, 0.2 and 0.5 GeV^2. The experimental design is optimized to extract the structure functions $P_{LL} - P_{TT}/\epsilon$ and P_{LT} and the electric and magnetic GPs of the proton, using the two analysis techniques at our disposal. These data will be obtained with competitive error bars and will be essential to build a consistent picture of the polarizabilities as a function of the distance scale.

3   Design of the experiment

The experiment will use the MAMI-C electron beam and the standard A1 setup [27]: the 5 cm long liquid hydrogen target and two spectrometers to detect in coincidence the outgoing electron and proton. These are the usual techniques in VCS experiments.

We have chosen to use spectrometers A and B only. Indeed, for the accurate measurement of $(ep \to ep\gamma)$ cross sections, we need to know the detector's acceptance to the 1-2% level. This is routinely achieved only for spectrometers A and B.

3.1 Guidelines

Data will be taken at three different Q^2, chosen in order to cover the region of interest between 0.1 and 0.5 GeV^2. The values are indicated by an arrow in Fig. 4. The kinematical settings have been studied using a detailed simulation developed for VCS [28]. The optimization was done according to the following guidelines:

- to be able to perform both LEX and DR analyses successfully on the data;

- to have a good sensitivity to both structure functions $P_{LL} - P_{TT}/\epsilon$ and P_{LT};

- to make use of the Out-Of-Plane capability of the A1 setup.

These items are developed in section 3.2.

3.2 Optimization

It is precious to have two different analysis techniques in VCS : LEX and DR (cf. section 1.3). We have designed the experiment in order to be able to make use of them both. Such a double analysis was performed at Bates and at JLab. It is also under way for the existing MAMI data at $Q^2 = 0.33$ GeV^2 [29].

We first define the "GP effect" as the relative deviation of $d^5\sigma_{exp}$ to $d^5\sigma_{BH+B}$:

$$[\text{GP effect}] = \frac{d^5\sigma_{exp} - d^5\sigma_{BH+B}}{d^5\sigma_{BH+B}} \quad . \tag{3}$$

In the LEX approach, truncating the expansion to the first order in q'_{cm}, this GP effect scales with q'_{cm} (cf. the explicit factor $\Phi q'_{cm}$ in front of the brackets in eq. 1). This term is always rather small ($\leq 20\%$) below the pion threshold. We want to select kinematics which maximize the GP effect, in order to measure it as precisely as possible. Consequently, to be able to use the LEX method efficiently, we choose an acceptance in q'_{cm} that is centered as high as possible below the pion threshold. Fig. 5 illustrates our choice.
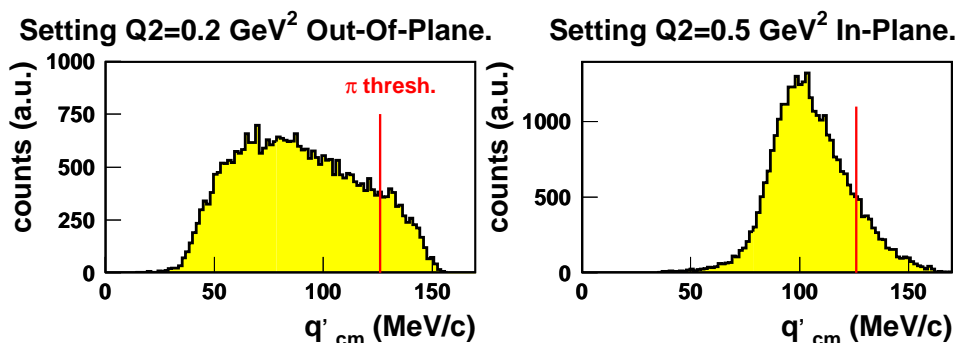
Figure 5: *Acceptance in q'_{cm} for two of the proposed settings. The LEX analysis can be done below the pion threshold of 126 MeV/c, the DR analysis can be done for all values of q'_{cm}.*

Also w.r.t. the LEX method, we want the higher-order term $\mathcal{O}(q'_{cm}{}^2)$ in eq. 1 to be small enough so that it can be neglected. To ensure that, one must try to estimate in advance the importance of this higher-order term. One way is to compare the "LEX" cross section:

$$d^5\sigma_{LEX} = d^5\sigma_{BH+B} + (\Phi q'_{cm}) \times \left[v_{LL} \cdot (P_{LL} - P_{TT}/\epsilon) + v_{LT} \cdot (P_{LT}) \right]$$

and the DR cross section $d^5\sigma_{DR}$ which takes into account all orders in q'_{cm}. The difference between the two represents the $\mathcal{O}(q'_{cm}{}^2)$ term. This comparison can be done at each point in phase space, provided that we fix the value of the structure functions which enter the calculation of the cross sections $d^5\sigma_{LEX}$ and $d^5\sigma_{DR}$. To this aim, we did a Q^2-interpolation between the (few) measured values of the structure functions. Table 1 shows our input values of $P_{LL} - P_{TT}/\epsilon$ and P_{LT} at each Q^2. (Λ_α) and (Λ_β) are the corresponding values of the free parameters in the DR model.

Table 1: *Input values of the structure functions for the design study.*

Q^2 (GeV^2)	$P_{LL} - P_{TT}/\epsilon$ (GeV^{-2})	P_{LT} (GeV^{-2})	(Λ_α) (GeV)	(Λ_β) (GeV)
0.1	42.5	-5.3	(0.85)	(0.70)
0.2	31.0	-4.0	(1.20)	(0.70)
0.5	10.7	-1.6	(1.00)	(0.70)

Then we performed a systematic study in order to select regions in the $(\theta_{\gamma\gamma cm}, \phi)$ phase space where $d^5\sigma_{LEX}$ and $d^5\sigma_{DR}$ agree well enough, thereby indicating that the $\mathcal{O}(q'_{cm}{}^2)$ term is small. The best region turns out to be a continuous band in $(\theta_{\gamma\gamma cm}, \phi)$, going from $\theta_{\gamma\gamma cm} \sim 100°$ at $\phi = 90°$, to the backward $\theta_{\gamma\gamma cm}$ angles at in-plane kinematics. This is illustrated by the green boxes in Fig. 6.

We find quite similar results for each Q^2. Based on that, we have defined **two spectrometer settings at each Q^2** :

1. **an out-of-plane setting** centered on $\phi = 90°$ and $\theta_{\gamma\gamma cm} = 100°$. At this central point, the coefficient v_{LT} in eq. 1 is numerically zero. Therefore this setting is essentially sensitive to the structure function $P_{LL} - P_{TT}/\epsilon$.

2. **an in-plane setting** centered on backward $\theta_{\gamma\gamma cm}$ angles. Strictly at $\theta_{\gamma\gamma cm} = 180°$, the coefficient v_{LL} is numerically zero and we are sensitive only to P_{LT}. Taking into account the full acceptance in $\theta_{\gamma\gamma cm}$, this second setting has the best mixed sensitivity to both structure functions.

To summarize, we have taken again the idea of the Bates experiment (i.e. a setting at $\phi = 90°$ sensitive to $P_{LL} - P_{TT}/\epsilon$, plus an in-plane setting sensitive to both structure functions) but we try to avoid a "breakdown of the LEX" due to the presence of a large $\mathcal{O}(q'_{cm}{}^2)$ term (a problem which happened in the Bates experiment).

Lastly, the kinematical settings were chosen in order to have the largest photon polarization ϵ. Again, this maximizes the GP effect. Typically, at fixed $(q_{cm}, q'_{cm}, \theta_{\gamma\gamma cm}, \phi)$, when one goes from $\epsilon = 0.6$ to $\epsilon = 0.9$ the GP effect is doubled. As a secondary impact, the counting rate increases with ϵ.
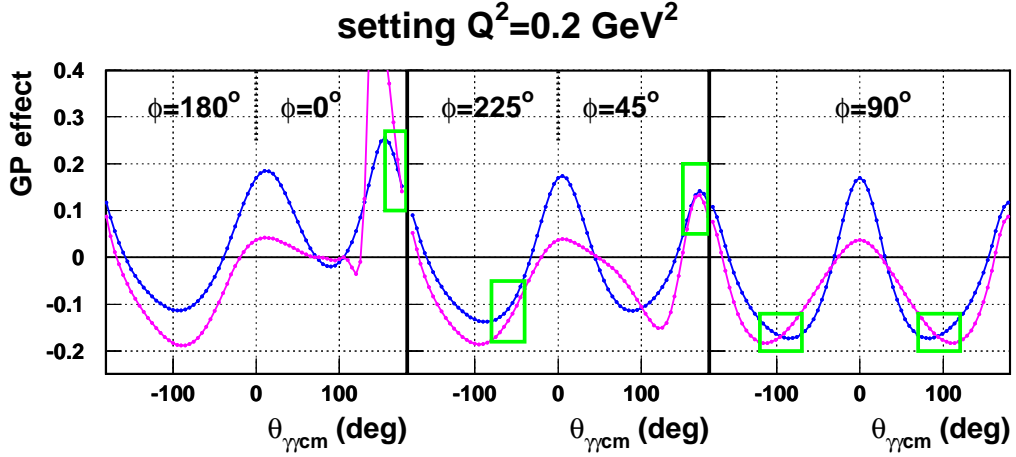
Figure 6: *The GP effect, calculated as $(d^5\sigma_{LEX} - d^5\sigma_{BH+B})/d^5\sigma_{BH+B}$ in magenta, and calculated as $(d^5\sigma_{DR} - d^5\sigma_{BH+B})/d^5\sigma_{BH+B}$ in blue, in different regions of $(\theta_{\gamma\gamma cm}, \phi)$. Kinematics are at $(q_{cm} = 458 \; MeV/c, \; q'_{cm} = 110 \; MeV/c, \; \epsilon = 0.85)$. The angle $\theta_{\gamma\gamma cm}$ is conventionally negative when ϕ belongs to the hemisphere [90°, 270°]. The structure functions are equal to $P_{LL} - P_{TT}/\epsilon = 31 \; GeV^{-2}$ and $P_{LT} = -4 \; GeV^{-2}$, in both LEX and DR calculations. The green boxes are where the LEX and DR effects are in good agreement (and large enough to be measured).*

The maximal values of ϵ that can be reached with the A1 setup are: $\epsilon = 0.90$, 0.85 and 0.62 at $Q^2 = 0.1$, 0.2, and 0.5 GeV^2 respectively (see table 3). The structure function $P_{LL} - P_{TT}/\epsilon$ will then be measured at a different ϵ for each Q^2, which is by no way a handicap from theoretical point of view.

4 Kinematical settings

Table 2: *The kinematical settings, out-of-plane ("oop") and in-plane ("inp"), for spectrometers A and B. (P_B, P_A) are the central momenta and (θ_B, θ_A) are the angles of the spectrometers w.r.t. the beam, in horizontal. OOPB is the out-of-plane angle of spectrometer B.*

setting name	particle in spectrometer	E_{beam} (MeV)	P_B ($\frac{MeV}{c}$)	θ_B (deg.)	OOPB (deg.)	P_A ($\frac{MeV}{c}$)	θ_A (deg.)
q2-0.1-oop	e' in spec.B	877	700	21.9	8.7	345	52.0
q2-0.1-inp	e' in spec.B	877	700	23.0	0.0	420	53.8
q2-0.2-oop	e' in spec.B	1005	784	29.1	7.3	489	52.3
q2-0.2-inp	e' in spec.B	1005	784	29.9	0.0	580	51.8
q2-0.5-oop	e' in spec.A	1035	740	38.7	8.0	647	51.0
q2-0.5-inp	e' in spec.A	1020	750	31.7	0.0	645	51.5

The experiment will be done in the standard way, detecting the outgoing electron and proton in the spectrometers and reconstructing the final photon by missing

mass. The high resolution of the A1 spectrometers ensures an excellent missing mass resolution, more than enough to separate the π^0 electroproduction events (which are always present in the acceptance). For the proposed kinematics the width of the missing mass squared peak of the VCS events is between 600 and 1000 MeV^2 (FWHM).

The tables of this section summarize the six settings chosen to measure the $ep \to ep\gamma$ cross section: table 2 presents the spectrometer settings and table 3 the main quantities of interest for the physics. As a side remark, one will note that the high values of ϵ (0.90, 0.85) are reached thanks to the MAMI-C energies, above 850 MeV. For the settings at $Q^2 = 0.5$ GeV^2 the proton momentum in the angular phase space of interest is too high for spectrometer A, therefore we choose to detect this particle in spectrometer B. Even with this option it is not possible to reach the backward values of $\theta_{\gamma\gamma cm}$. Therefore, we have chosen an in-plane setting centered on less backward angles: $\theta_{\gamma\gamma cm} = 100°$. According to Fig. 6, the LEX and DR polarizability effect are in less good agreement in this region. Therefore one may expect different results from LEX and DR analyses for this setting, as has been observed already in other experiments [29].

Lastly, when the out-of-plane angle OOPB is not zero, and especially at the lowest Q^2, it is mandatory to displace the average transverse beam position w.r.t. the target center, to avoid that the "spectrometer B" particle hits the upper part of the target holder frame. Typical beam offsets needed at $Q^2 = 0.1$ GeV^2 are 2 mm down and 2 mm towards spectrometer B. Exact values can be provided by the simulation.

Table 3: *Some physical variables of interest for each kinematical setting. We give values averaged over the acceptance, and in brackets the range covered in the acceptance, for the variables which will be binned in the analysis.*

setting name	Q^2 (GeV^2)	$\tilde{Q}^2$	ϵ	q_{cm} (MeV/c)	q'_{cm}	$\theta_{\gamma\gamma cm}$ (deg.)	ϕ (deg.)
q2-0.1-oop	0.10	0.10	0.90	322	100 [60,150]	100 [70,140]	90 [60,120]
q2-0.1-inp	0.10	0.10	0.90	322	100 [60,150]	150 [125,180]	- - [0,360]
q2-0.2-oop	0.21	0.20	0.85	458	95 [40,150]	100 [60,150]	90 [60,120]
q2-0.2-inp	0.21	0.20	0.85	458	95 [40,150]	150 [115,180]	- - [0,360]
q2-0.5-oop	0.50	0.45	0.62	757	100 [40,180]	100 [40,150]	90 [60,150]
q2-0.5-inp	0.50	0.45	0.62	757	100 [70,150]	100 [50,140]	180 [130,230]

In table 3, $\tilde{Q}^2$ is a variable specific to VCS. It is defined as the four-momentum transfer Q^2 taken in the limit $q'_{cm} \to 0$, at fixed q_{cm}. The structure functions and the GPs depend on this $\tilde{Q}^2$. Since we are near the reaction threshold, $\tilde{Q}^2$ is always close to the experimental Q^2.

Table 4 gives the order of magnitude of the effect we want to measure. It is 10-20% of the cross section at the highest q'_{cm} below the pion threshold. Of course, the larger the GP effect, the smaller the impact of systematic errors on the error on the physics observables. Figure 7 shows a detailed example of the GP effect as a function of $\theta_{\gamma\gamma cm}$. For the out-of-plane setting there is practically no contribution due to P_{LT}. It is the in-plane measurement which allows to measure it.

Setting Q2 = 0.2 GeV^2 Out-Of-Plane
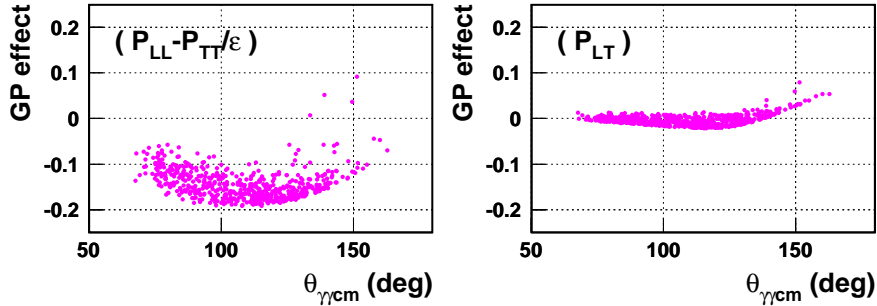
Setting Q2 = 0.2 GeV^2 In-Plane
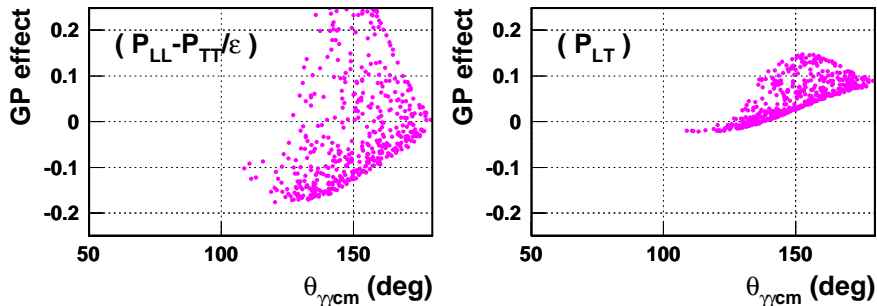
Figure 7: *The GP effect, calculated as $(d^5\sigma_{LEX} - d^5\sigma_{BH+B})/d^5\sigma_{BH+B}$, plotted separately for the first (left) and second (right) structure function, for the settings at $Q^2 = 0.2$ GeV^2: out-of-plane (top) and in-plane (bottom). Events are selected at $q'_{cm} = 110 \pm 1$ MeV/c.*

5   Event rate estimates and beamtime

Table 5 summarizes the various count rate estimates. The beam current has been set in order to keep an acquisition deadtime below $\sim 20\%$. The VCS coincidence rate is calculated using our Monte-Carlo simulation. The signal-to-background ratio (S/B) is calculated for events satisfying all main analysis cuts, and is always very good. The desired VCS statistics is deduced from our simulated LEX fit (see next section) and the projected errors of table 6. The beamtime indicated in the table is the one needed to achieve this number of VCS events.

For each setting an extra-beamtime of about 1.5 day has to be added in order to conduct a series of calibration runs, among which:

- trigger efficiency runs

- sieve-slit and thin foil runs for spectrometer optics

- empty target runs

- VCS at very low q'_{cm} (~ 30 MeV/c) to measure the $ep \rightarrow ep\gamma$ cross section and verify the agreement with the (BH+B) calculation.

10

Table 4: *The $ep \to ep\gamma$ cross section (BH+B part) averaged over the acceptance, and the GP effect as defined in eq. 3. This quantity is calculated using the LEX formula (eq. 1) and the structure functions of table 1. We give first the global GP effect, then the separate effect of each structure function, for events at one single $q'_{cm} = 110\,\mathrm{MeV}/c$. In brackets is the range covered in the acceptance for this q'_{cm}.*

setting name	$d^5\sigma$ (pb /MeV /sr^2)	GP effect global		GP effect due to $P_{LL} - P_{TT}/\epsilon$		GP effect due to P_{LT}	
q2-0.1-oop	1.8	-16%	[-20,-10]%	-16%	[-20,-10]%	0%	[-2, +2]%
q2-0.1-inp	1.0	- -	[-20,+20]%	- -	[-20,+20]%	+10%	[0,+20]%
q2-0.2-oop	1.0	-17%	[-20,-10]%	-17%	[-20,-10]%	0%	[-2, +2]%
q2-0.2-inp	0.6	- -	[-18,+20]%	- -	[-18,+20]%	+10%	[0, +15]%
q2-0.5-oop	0.12	-12%	[-14, -8]%	-12%	[-14, -8]%	0%	[-2 , +2]%
q2-0.5-inp	0.07	-12%	[-14,-10]%	-17%	[-19,-13]%	+5%	[+4, +6]%

Table 5: *Event rates, beam current, desired statistics and beamtime. The rates are estimated for a hydrogen target of 50 mm length and the given beam current.*

setting name	Beam Curr. (μA)	single rate in B (Hz)	single rate in A (Hz)	total coinc. rate (Hz)	VCS coinc. rate (Hz)	S/B ratio	desired number of VCS events	beam time request
q2-0.1-oop	5	10k (e)	64k	67	1.2	5	150k	50 h
q2-0.1-inp	8	17k (e)	36k	62	2.0	9	450k	100 h
q2-0.2-oop	10	13k (e)	45k	64	3.7	15	600k	70 h
q2-0.2-inp	11	15k (e)	40k	63	3.8	21	900k	100 h
q2-0.5-oop	20	9k	9k (e)	9	1.2	63	360k	130 h
q2-0.5-inp	20	13k	9k (e)	12	0.4	25	120k	130 h

The total beamtime requested is thus of 800 hours, using the electron beam of MAMI-C (unpolarized) at an energy between 870 and 1040 MeV.

6 Projected errors on the VCS observables

In order to estimate the error bars on $P_{LL} - P_{TT}/\epsilon$ and P_{LT} (or the GPs) than can be reached in the experiment, we have simulated the extraction of these observables from the data. This is done by generating pseudo-measured cross sections at the proposed kinematics, and performing a fit on these data, of the LEX type or DR type.

A LEX fit is fast to design, and could be done during the writing of this proposal. A DR fit is much longer to perform (due to computing time) and has not been done yet; nevertheless some conclusions can be extrapolated from LEX to DR analysis.

6.1 Simulation of a LEX extraction of the structure functions

For each kinematical setting we define a 3D-binning in q'_{cm}, $\theta_{\gamma\gamma cm}$ and ϕ. In each bin we generate a pseudo-cross section $d^5\sigma(ep \to ep\gamma)$ which includes a first-order GP effect (according to eq. 1). The statistical error bar on this cross section follows the statistics in the bin, as given by our VCS Monte-Carlo simulation.

For the in-plane settings at backward angles, we restrict the analysis to a small angular region where the LEX and DR calculations agree rather well, to have a guarantee that the LEX truncation of eq. 1 works.

Then, at each Q^2 we perform a "LEX fit", on the two settings together: out-of-plane and in-plane. The deviation of $d^5\sigma_{exp}$ to $d^5\sigma_{BH+B}$ is fitted as a linear combination of $P_{LL} - P_{TT}/\epsilon$ and P_{LT}, using a χ^2-minimization. The statistical error bar on the parameters is deduced from the fit. In this way we can determine for each setting the number of VCS events required to produce a given statistical error on $P_{LL} - P_{TT}/\epsilon$ and P_{LT}. Fig. 8 summarizes the results of this simulation. They correspond to the VCS statistics indicated in table 5.
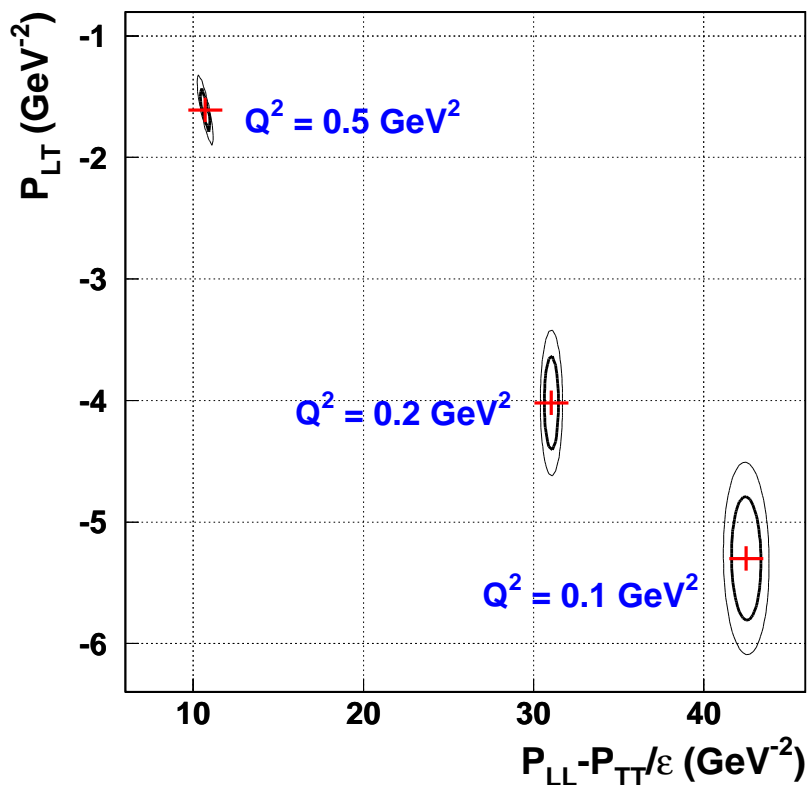
Figure 8: *Results of our simulated LEX fit of the structure functions. The input values (red crosses) are the ones given in table 1. The thick ellipse is the contour at $(\chi^2_{min}+1)$, which gives CL=70% for each parameter independently. The thin ellipse is the contour at $(\chi^2_{min}+2.41)$, which gives CL=70% for both parameters simultaneously [30].*

This simulation procedure can also provides a rough estimate of the systematic error on the observables. To this aim we re-do the LEX fit with cross sections changed systematically by some amount. Here we have considered an uncertainty of $\pm 1.5\%$ in the global normalisation, which is applied to all cross-section points in the same way.

6.2 Results

Table 6 shows our estimate of the error bars on the structure functions for the proposal, together with the results of the previous VCS experiments. To complete this table, we can extrapolate our simulated LEX results to DR ones: in this latter case the statistical error will be smaller (because the DR fit includes all VCS events without restriction) and we expect the systematic error to be comparable to the LEX one.

From table 6 it is obvious that at MAMI we can reach very small statistical error bars. As in the other experiments (except Bates) the systematic error will be the dominant one. To estimate this systematic error in the proposal, we have considered a $\pm 1.5\%$ uncertainty in the global normalisation of the cross sections. This value is already hard to achieve; for example, the radiative corrections to VCS, which contribute to the global normalization, are not known to better than 1%.

Table 6: *VCS experiments: published results on the structure functions, and projected errors for the proposed experiment. The first error is statistical, the second is systematic. The statistical error corresponds to a confidence level CL=70% on each structure function, independently of the other. For the proposal the errors are deduced from our simulated LEX fit of section 6.1.*

Experiment	Q^2 (GeV^2)	$P_{LL} - P_{TT}/\epsilon$ (GeV^{-2})			P_{LT} (GeV^{-2})			type of analysis
Bates [6]	0.06	54.5	$\pm$ 4.8	$\pm$ 2.0				LEX
		46.7	$\pm$ 4.9	$\pm$ 2.0	-8.9	$\pm$ 4.2	$\pm$ 0.8	DR
Proposal	**0.10**	——	$\pm$ 1.0	$\pm$ 3.7	——	$\pm$ 0.6	$\pm$ 1.5	**LEX**
Proposal	**0.20**	——	$\pm$ 0.5	$\pm$ 3.7	——	$\pm$ 0.4	$\pm$ 0.9	**LEX**
MAMI [4]	0.33	23.7	$\pm$ 2.2	$\pm$ 4.3	-5.0	$\pm$ 0.8	$\pm$ 1.8	LEX
MAMI [5]	0.33	27.1	$\pm$ 1.9	$\pm$ 3.0	-8.0	$\pm$ 0.7	$\pm$ 2.2	LEX
Proposal	**0.50**	——	$\pm$ 0.4	$\pm$ 1.8	——	$\pm$ 0.2	$\pm$ 0.3	**LEX**
JLab [7]	0.92	1.77	$\pm$ 0.24	$\pm$ 0.70	-0.56	$\pm$ 0.12	$\pm$ 0.17	LEX
		1.70	$\pm$ 0.21	$\pm$ 0.89	-0.36	$\pm$ 0.10	$\pm$ 0.27	DR
					-0.71	$\pm$ 0.07	$\pm$ 0.05	DR
JLab [7]	1.76	0.54	$\pm$ 0.09	$\pm$ 0.20	-0.04	$\pm$ 0.05	$\pm$ 0.06	LEX
		0.40	$\pm$ 0.05	$\pm$ 0.16	-0.09	$\pm$ 0.02	$\pm$ 0.03	DR

• Projected errors on the electric and magnetic GPs

As explained in section 1.3, the electric and magnetic GPs are most directly obtained by doing a DR analysis on the measured cross sections. In the LEX method they are determined less directly. Even without having simulated a DR analysis for the proposed experiment, we can state that the expected error bar on α_E and β_M will be small and largely competitive w.r.t. to existing measurements. This follows

from the good accuracy expected on the measurement of the structure functions, see table 6.

It should be noted that precise measurements of the proton form factors G_E^p, G_M^p at low Q^2 [31] will improve the determination of the VCS observables. Indeed the GP effect is always measured by a deviation to the Bethe-Heitler+Born cross section, which depends intrinsically on these form factors.

We would like to conclude by pointing out that MAMI with its A1 equipment provides unique conditions to perform the proposed experiment successfully. Actually it is the only laboratory in the world where this experiment can be achieved.

References

[1] V. Olmos de Leon, et al., Low-energy Compton scattering and the polarizabilities of the proton, Eur. Phys. J. A10 (2001) 207–215.

[2] H. Arenhövel, D. Drechsel, Generalized nuclear polarizabilities in (e,e'γ) coincidence experiments, Nucl. Phys. A233 (1974) 153.

[3] P. A. M. Guichon, G. Q. Liu, A. W. Thomas, Virtual Compton scattering and generalized polarizabilities of the proton, Nucl. Phys. A591 (1995) 606–638.

[4] J. Roche, et al., The first determination of generalized polarizabilities of the proton by a virtual Compton scattering experiment, Phys. Rev. Lett. 85 (2000) 708–711.

[5] P. Janssens, et al., A new measurement of the structure functions $P_{LL} - P_{TT}/epsilon$ and P_{LT} in virtual Compton scattering at $Q^2 = 0.33$ (GeV/c)^2, Eur. Phys. J. A37 (2008) 1–8.

[6] P. Bourgeois, et al., Measurements of the generalized electric and magnetic polarizabilities of the proton at low Q^2 using the VCS reaction, Phys. Rev. Lett. 97 (2006) 212001.

[7] G. Laveissière, et al., Measurement of the generalized polarizabilities of the proton in virtual Compton scattering at $Q^2 = 0.92$ GeV^2 and 1.76 GeV^2, Phys. Rev. Lett. 93 (2004) 122001.

[8] G. Q. Liu, A. W. Thomas, P. A. M. Guichon, Virtual Compton scattering from the proton and the properties of nucleon excited states, Austral. J. Phys. 49 (1996) 905–918.

[9] B. Pasquini, S. Scherer, D. Drechsel, Generalized polarizabilities of the proton in a constituent quark model revisited, Phys. Rev. C63 (2001) 025205.

[10] A. Metz, D. Drechsel, Generalized polarizabilities of the nucleon studied in the linear sigma model, Z. Phys. A356 (1996) 351–357.

[11] A. Metz, D. Drechsel, Generalized polarizabilities of the nucleon studied in the linear sigma model. II, Z. Phys. A359 (1997) 165–172.

[12] M. Vanderhaeghen, Virtual Compton scattering study below pion production threshold, Phys. Lett. B368 (1996) 13–19.

[13] A. Y. Korchin, O. Scholten, Nucleon polarizabilities in virtual Compton scattering, Phys. Rev. C58 (1998) 1098–1100.

[14] T. R. Hemmert, B. R. Holstein, G. Knochlein, S. Scherer, Virtual Compton scattering off the nucleon in chiral perturbation theory, Phys. Rev. D55 (1997) 2630–2643.

[15] T. R. Hemmert, B. R. Holstein, G. Knochlein, S. Scherer, Generalized polarizabilities and the chiral structure of the nucleon, Phys. Rev. Lett. 79 (1997) 22–25.

[16] T. R. Hemmert, B. R. Holstein, G. Knochlein, D. Drechsel, Generalized polarizabilities of the nucleon in chiral effective theories, Phys. Rev. D62 (2000) 014013.

[17] C. W. Kao, M. Vanderhaeghen, Generalized spin polarizabilities of the nucleon in heavy baryon chiral perturbation theory at next-to-leading order, Phys. Rev. Lett. 89 (2002) 272002.

[18] C.-W. Kao, B. Pasquini, M. Vanderhaeghen, New predictions for generalized spin polarizabilities from heavy baryon chiral perturbation theory, Phys. Rev. D70 (2004) 114004.

[19] D. Djukanovic, PhD Thesis, Mainz (2008); D. Djukanovic, B. Pasquini, S. Scherer, in preparation.

[20] B. Pasquini, M. Gorchtein, D. Drechsel, A. Metz, M. Vanderhaeghen, Dispersion relation formalism for virtual Compton scattering off the proton, Eur. Phys. J. A11 (2001) 185–208.

[21] D. Drechsel, B. Pasquini, M. Vanderhaeghen, Dispersion relations in real and virtual Compton scattering, Phys. Rept. 378 (2003) 99–205.

[22] C. E. Hyde-Wright, K. de Jager, Electromagnetic form factors of the nucleon and compton scattering, Ann. Rev. Nucl. Part. Sci. 54 (2004) 217–267.

[23] N. d'Hose, Virtual Compton scattering at MAMI, Eur. Phys. J. A28 (2006) 117–127.

[24] P. A. M. Guichon, M. Vanderhaeghen, Virtual Compton scattering off the nucleon, Prog. Part. Nucl. Phys. 41 (1998) 125–190.

[25] D. Drechsel, O. Hanstein, S. S. Kamalov, L. Tiator, A unitary isobar model for pion photo- and electroproduction on the proton up to 1 GeV, Nucl. Phys. A645 (1999) 145–174.

[26] J. Friedrich, T. Walcher, A coherent interpretation of the form factors of the nucleon in terms of a pion cloud and constituent quarks, Eur. Phys. J. A17 (2003) 607–623.

[27] K. I. Blomqvist, et al., The three-spectrometer facility at the Mainz microtron MAMI, Nucl. Instrum. Meth. A403 (1998) 263–301.

[28] P. Janssens, et al., Monte Carlo simulation of virtual Compton scattering below pion threshold, Nucl. Instr. Meth. A566 (2006) 675–686.

[29] H.Fonvieille (for the MAMI-A1 Collaboration), work in progress.

[30] MINUIT Reference Manual, Cern program Library Long Writeup D506 (1992).

[31] M.O.Distler, Proposal, MAMI A1-2/05 (2005).